

Tokyo, Japan Oct. 31-Nov. 2, 1988

TELE-EXISTENCE SIMULATOR WITH ARTIFICIAL REALITY (1)

- DESIGN AND EVALUATION OF A BINOCULAR VISUAL DISPLAY USING SOLID MODELS -

Susumu Tachi, Hirohiko Arai, and Taro Maeda

Mechanical Engineering Laboratory, MITI
Tsukuba Science City, Ibaraki 305 Japan

Abstract

In this paper, extension of tele-existence technology to the artificially constructed environment is sought. A visual tele-existence simulator is designed, pseudo-real-time solid-model robot simulator with binocular three dimensional display function is made, and its feasibility is experimentally evaluated.

Introduction

Tele-existence [1,2] aims at a natural and efficient remote control of robots by providing an operator a real time sensation of presence. It is an advanced type of teleoperation system that enables a human operator at the controls to perform remote manipulation tasks dexterously with the feeling that he or she exists in one of the remote anthropomorphic robots in the several remote environments. Similar concept is called artificial reality [3] or telepresence [4] in the United States.

In the previous reports [1,2], the principle of the tele-existence sensory display was proposed. Its design procedure was explicitly defined. Experimental visual display hardwares were made, and the feasibility of the visual display with the sensation of presence was demonstrated by psychophysical experiments using the test hardwares. A method was also proposed to realize a mobile tele-existence system, which can be remotely driven with the auditory and visual sensation of presence. A prototype mobile tele-vehicle system was constructed and the feasibility of the method was evaluated. The effectiveness of the proposed system was evaluated by navigation experiments of the mobile robot through an obstructed space [5]. The principle of the active power assistance [6] was applied for controlling the visual display with two degrees of freedom.

In this paper, extension of the tele-existence to the artificially constructed environmental information is sought, the visual tele-existence simulator is designed, pseudo-real-time binocular solid model robot simulator is made, and its feasibility is experimentally evaluated.

Two main situations for the simulator usages are:

(1) To provide the operator information of the remote environment which human senses do not work but the robot's sensors do. For example, at night infrared sensor information is converted to visible light to see an object in the dark. It is also possible to superimpose range information gathered by the robot's ultrasonic and/or laser range sensors to the three dimensional visual display. The operator can effectively use this piece of information to augment human ability.

(2) To provide totally artificial but realistic environmental information to the operator, e.g., realization of virtual terminal or virtual console for the operator [3]. The operator can enjoy variety of consoles without changing them physically. This can also be used for the simulation study for training and also for optimal parameter selection and evaluation of man-machine system. The usage of the system as scientific tools for the analysis of human visual sensation, motion control and sensor-motor coordination is also possible.

As the first step toward the goal, a solid model robot manipulator with pseudo-real-time shading capability was constructed. By using the specially designed binocular optical system, three dimensional observation, which can exactly assign the distance and the size of the manipulator and an object, became possible.

In this paper, the design method and the effectiveness of the binocular presentation and also the effect of the use of the solid model compared with the use of the wire-frame model are quantitatively evaluated.

Pseudo-Real-Time Robot Simulator System

The test hardware system consists of posture measurement subsystem, computation subsystem, solid model subsystem and binocular vision subsystem as is shown in Fig. 1.

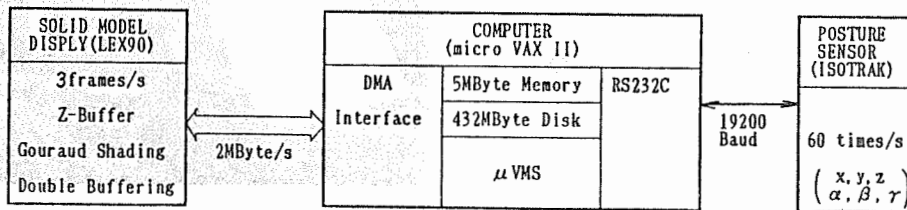


Fig. 1 Schematic diagram of the robot simulator.

The posture measurement subsystem measures the operator's wrist position and orientation in real time (60 Hz) using electromagnetic sensor (3SPACE TRACKER). This consists of a 3-axis field source and a similarly constructed 3-axis field sensor (fig. 2). The field source's three orthogonal axes are sequentially excited with a 10 kHz carrier, which produces three corresponding orthogonal AC magnetic fields. Signals that carry the information on the location and orientation of the sensor relative to the source are induced in the three axes of the sensor which is placed in the magnetic fields. The sensor outputs are filtered, synchronously detected and digitized to produce nine measurements. The computer processes these measurements to determine the three position coordinates and three directional cosines of the sensor relative to the source. Positional accuracy is 2.5 mm and angular accuracy is 0.5 degrees in ± 1.5 m cubic measurement field.

The measured coordinates (x,y,z) and directional cosines (α, β, γ) are sent to the computation subsystem (micro VAX II) via RS232C (19,200 baud).

A solid model of the direct drive (DD) manipulator of the authors' laboratory, of which analytical inverse kinematic solution is obtained, was made in the computation subsystem. The configuration of the manipulator (R-P-P-P-P-R) is shown in Fig. 3. The solid model of each link is made by a prism with an equilateral duodegon base, which approximates cylinder when Gouraud shaded. Each link is represented by a 4×200 matrix of the vertices whose origin is fixed to the link.

The computation subsystem calculates the inverse kinematics of the manipulator of which solid model is stored in the memory of the subsystem in order to determine the joint angles of the manipulator ($\theta_1, \theta_2, \theta_3, \theta_4, \theta_5, \theta_6$). The subsystem determines the coordinates of the solid model manipulator with reference to the world frame by using homogeneous transformation. Figure 3 shows the homogeneous transformation used to get the display data matrix from the model data and estimated joint angles. It also determines the shading information at vertices. Then perspective projections on the left and right display fields of the display plane are performed. These pieces of information are sent to the solid model display subsystem (LEX 90) via DMA interface (2 Mbyte/s).

The solid model display subsystem conducts Gouraud shading of each polygon and hidden surface elimination is done quickly by using Z-buffer. Double buffering technique is implemented so that the complete shaded

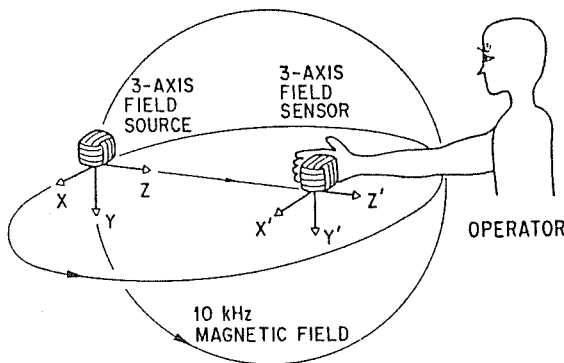
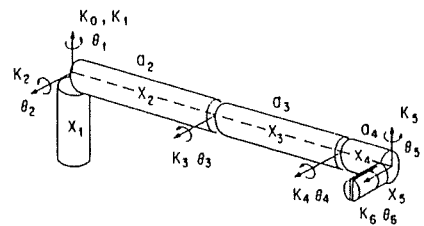


Fig. 2 Magnetic measurement of a human movement.

picture is always displayed. The display rate of 1 frames per second is attained for the whole manipulator with 6 degrees of freedom with a hand and 3 frames per second when only the hand portion is displayed.

The binocular vision subsystem consists of two mirrors and two lenses. It is designed to give the same disparities and visual angles on the retinae of a human operator when observed by the human operator binocularly, which means the operator observes the object at the same distance where the object is supposed to be with the same object size with reference to the world frame.

A general view of the simulator is shown in Fig. 4.



X_1, \dots, X_5 model data matrix of 4×200 (X_1, X_2 : BACKWARD)
 Z_1, \dots, Z_5 display data matrix of 4×200 (X_3, X_4, X_5 : FORWARD)

$$\begin{matrix}
 A_1 = \begin{bmatrix} C_1 & 0 & S_1 & 0 \\ S_1 & 0 & -C_1 & 0 \\ 0 & 1 & 0 & 0 \\ 0 & 0 & 0 & 1 \end{bmatrix} &
 A_2 = \begin{bmatrix} C_2 & -S_2 & 0 & C_2 a_2 \\ S_2 & C_2 & 0 & S_2 a_2 \\ 0 & 0 & 1 & 0 \\ 0 & 0 & 0 & 1 \end{bmatrix} &
 A_3 = \begin{bmatrix} C_3 & -S_3 & 0 & C_3 a_3 \\ S_3 & C_3 & 0 & S_3 a_3 \\ 0 & 0 & 1 & 0 \\ 0 & 0 & 0 & 1 \end{bmatrix} &
 V: \text{perspective transform} \\
 A_4 = \begin{bmatrix} C_4 & 0 & -S_4 & C_4 a_4 \\ S_4 & 0 & C_4 & S_4 a_4 \\ 0 & -1 & 0 & 0 \\ 0 & 0 & 0 & 1 \end{bmatrix} &
 A_5 = \begin{bmatrix} C_5 & 0 & S_5 & 0 \\ S_5 & 0 & -C_5 & 0 \\ 0 & 1 & 0 & 0 \\ 0 & 0 & 0 & 1 \end{bmatrix} &
 A_6 = \begin{bmatrix} C_6 & -S_6 & 0 & 0 \\ S_6 & C_6 & 0 & 0 \\ 0 & 0 & 1 & 0 \\ 0 & 0 & 0 & 1 \end{bmatrix} &
 \theta_1, \dots, \theta_6 \text{ measured variables}
 \end{matrix}$$

$$\begin{aligned}
 Z_1 &= VX_1, & Z_2 &= VA_1 A_2 X_2, & Z_3 &= VA_1 A_2 A_3 X_3, \\
 Z_4 &= VA_1 A_2 A_3 A_4 X_4, & Z_5 &= VA_1 A_2 A_3 A_4 A_5 X_5
 \end{aligned}$$

Fig. 3 Configuration of the solid model of the manipulator.

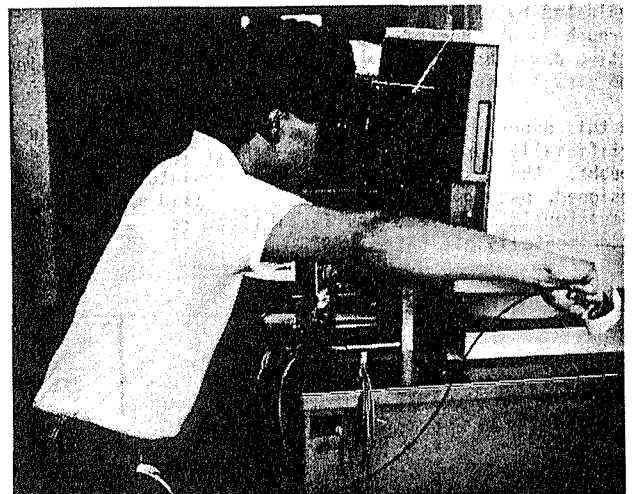


Fig. 4 General view of the binocular solid model robot simulator.

Binocular Display Design

One of the most important features of the three-dimensional display is that we can present an image of an object in front of a human operator at the distance where the real object is supposed to be located keeping the apparent size of the displayed object as exactly the same size of the original object. An arbitrary position and orientation can also be chosen.

In order to attain a three-dimensional display system with the above mentioned function, it is necessary to design the system which satisfies the following psychophysical relation adding to the conventional design of disparity between right and left corresponding points.

$$\text{Perceived Size} \propto \text{Visual Angle} \times \text{Distance}$$

where Perceived Size is a perceived (subjective) size of an object, Visual Angle is a visual angle or size of the human retinal image, and Distance is a distance from a human observer to the object. This means perceived size of the observed object is kept constant inspite of the change of distance in an appropriate distance range. This is known as size constancy.

First solid model of an object is represented by the coordinate which is attached to the object ($O'-X'Y'Z'$). This is described by the real scale, i.e., it is realized as a life-sized model in the computer. Figure 5 shows the relation.

Next we assign the location and orientation of the object relative to the observer-centered coordinate ($O-XYZ$). Then we transform the coordinate of the object as is located at the assigned position (${}^A P_{BORG}$) with the assigned orientation (${}^A R$) relative to the observer-centered coordinate by using the following homogeneous transformation:

$$\begin{pmatrix} X_i, \dots, X_n \\ Y_i, \dots, Y_n \\ Z_i, \dots, Z_n \\ W_i, \dots, W_n \end{pmatrix} = \begin{pmatrix} {}^A R & {}^A P_{BORG} \\ 0 & 0 & 0 & 1 \end{pmatrix} \begin{pmatrix} x'_i, \dots, x'_n \\ y'_i, \dots, y'_n \\ z'_i, \dots, z'_n \\ 1, \dots, 1 \end{pmatrix}$$

$$x_i = \frac{X_i}{W_i}, y_i = \frac{Y_i}{W_i}, z_i = \frac{Z_i}{W_i} \quad (i=1, \dots, n)$$

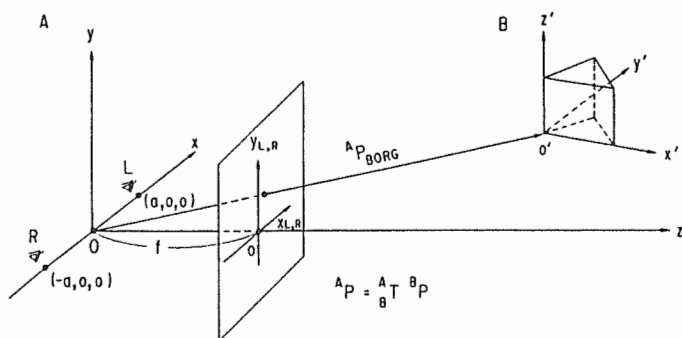


Fig. 5 Representation of the model and the space.

Perspective transformations, which project the object onto the display (CRT) plane which is perpendicular to the Z-axis at the distance of f from the origin O, should be conducted for the left and right eyes. However, direct transformations yield an overlapped images. It is, therefore, necessary to use modified transformation which separate the transformed images on the display plane, and correct them to the original right transformation using the optical apparatus shown in Fig. 6. Four mirrors in the apparatus correct the perspective transformation.

Ideally the distance to the virtual plane (dvir) where the human observer observes the images, which fuse to give the natural three-dimensional sensation, should be controlled to coincide with the distance to the object (${}^A P_{BORG}$) controlling optical parameters of the apparatus. However, experiments revealed that if $200 \text{ mm} < {}^A P_{BORG} < \infty$, dvir can be fixed to 1000 mm, and if $145 \text{ mm} < {}^A P_{BORG} < 2000 \text{ mm}$, dvir can be fixed to 500 mm. This makes the design and realization of the system more practical [5].

In this system convex lenses with the focal length of 282 mm are used to fix the distance to the virtual plane 500 mm.

Field angle for each eye is 42.5 degrees as is shown in Fig. 6.

The following homogeneous transformations are used. In the transform all parameters are described according to their physical dimension. Therefore, transform from physical parameters to device oriented parameters was also conducted (the distance between pixcells is 0.5 mm in this case).

$$\begin{pmatrix} X'_i, \dots, X'_n \\ Y'_i, \dots, Y'_n \\ Z'_i, \dots, Z'_n \\ W'_i, \dots, W'_n \end{pmatrix} = \begin{pmatrix} 1 & 0 & 0 & a+s \\ 0 & 1 & 0 & 0 \\ 0 & 0 & 1 & 0 \\ 0 & 0 & 0 & 1 \end{pmatrix} \begin{pmatrix} 1 & 0 & 0 & 0 \\ 0 & 1 & 0 & 0 \\ 0 & 0 & 1 & 0 \\ 0 & 0 & 1/f & 0 \end{pmatrix} \begin{pmatrix} 1 & 0 & 0 & -a \\ 0 & 1 & 0 & 0 \\ 0 & 0 & 1 & 0 \\ 0 & 0 & 0 & 1 \end{pmatrix} \begin{pmatrix} x_i, \dots, x_n \\ y_i, \dots, y_n \\ z_i, \dots, z_n \\ 1, \dots, 1 \end{pmatrix}$$

$$= \begin{pmatrix} 1 & 0 & \frac{a+s}{f} & -a \\ 0 & 1 & 0 & 0 \\ 0 & 0 & 1 & 0 \\ 0 & 0 & 1/f & 0 \end{pmatrix} \begin{pmatrix} x_i, \dots, x_n \\ y_i, \dots, y_n \\ z_i, \dots, z_n \\ 1, \dots, 1 \end{pmatrix} \begin{cases} x'_i = \frac{X'_i}{W'_i} \\ y'_i = \frac{Y'_i}{W'_i} \\ z'_i = \frac{Z'_i}{W'_i} \end{cases} \quad (i=1, \dots, n)$$

$$\begin{pmatrix} X''_i, \dots, X''_n \\ Y''_i, \dots, Y''_n \\ Z''_i, \dots, Z''_n \\ W''_i, \dots, W''_n \end{pmatrix} = \begin{pmatrix} 1 & 0 & -\frac{a+s}{f} & a \\ 0 & 1 & 0 & 0 \\ 0 & 0 & 1 & 0 \\ 0 & 0 & 1/f & 0 \end{pmatrix} \begin{pmatrix} x_i, \dots, x_n \\ y_i, \dots, y_n \\ z_i, \dots, z_n \\ 1, \dots, 1 \end{pmatrix} \begin{cases} x''_i = \frac{X''_i}{W''_i} \\ y''_i = \frac{Y''_i}{W''_i} \\ z''_i = \frac{Z''_i}{W''_i} \end{cases} \quad (i=1, \dots, n)$$

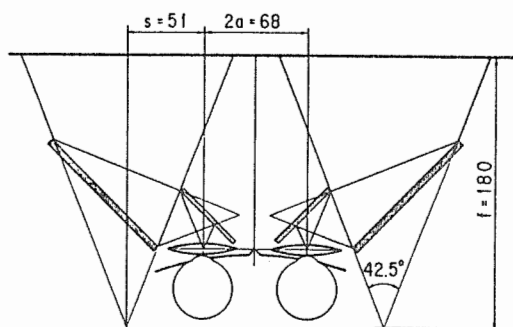


Fig. 6 Binocular display unit.

Experiments

Effect of Binocular Vision

(1) Objective In order to evaluate the effect of binocular presentation quantitatively, a following experiment of object handling was conducted using the simulator. The object is a rectangular prism with a base 50 mm x 50 mm and a height of 70 mm, which is represented as a wire-frame model as is shown in Fig. 7. The frontal surface has a mark on it to be identified. The object was located at the location 500 mm ± 50 mm in front of an operator randomly. The orientation of the object also varied randomly within the range of ± 0.75 rad in all three directions deviated from the central position. The operator was asked to adjust the position and the orientation of the displayed manipulator so that they coincide with the random position and orientation of the object, respectively. The displayed manipulator is controlled to follow the operator's arm movement by the measurement system explained in the previous section. The operator tries to control the normal vector \vec{h}_z to coincide with the normal vector \vec{O}_z , the axis h_x with the axis O_x , and the center of gravity (X_h, Y_h, Z_h) with (X_o, Y_o, Z_o) . In this experiment interference between the object and the manipulator is ignored so that the operator can control the position and orientation of the manipulator from any direction penetrating the object. Although a frame rate was 3 frames per second with double buffering, appropriate feeling of movement was attained because no shutter was used and the scene had no fluttering.

(2) Display Schemes Compared display schemes are divided into two main classes, i.e., binocular display (the manipulator and the object's sizes, positions and orientations are displayed in life-size) and monocular display (the same condition as in the case of the binocular display except the same image is presented to both eyes of the operator). Adding to the above classification, schemes are divided into sub-groups according to the following auxiliary cues which are used to enhance the distance (range) information.

(a) The range difference between the object's center and the hand's center is displayed in figures (numerals in mm).
 (b) The range difference is expressed in bar-graph.
 (c) The range difference is expressed as the frequency difference of presented tone. Range-frequency conversion is done according to the following formula: $f = f_0 \exp(-\lambda \Delta d)$, where $f_0 = 4167$ Hz and $\lambda = 0.01$. The tone is presented as a tone burst with 180 ms of presentation period and 50 ms of rest period in order to avoid auditory adaptation. Figure 8 shows a display example. Both the numerals and the bar-graphs are displayed at the position of infinity for both binocular and monocular display schemes.

(3) Criteria for Comparison The following formula is used for the comparison of the display schemes:

$$\Delta d = \sqrt{(X_o - X_h)^2 + (Y_o - Y_h)^2 + (Z_o - Z_h)^2}$$

$$\Delta \theta = \cos^{-1}(\vec{O}_z \cdot \vec{h}_z)$$

$$\Delta \phi = \cos^{-1}\left(\frac{\vec{O}_z \times \vec{h}_z}{|\vec{O}_z \times \vec{h}_z|} \cdot \vec{O}_x\right) - \frac{\pi}{2}$$

where Δd is the range error, $\Delta \theta$ is the angular error between two normal vectors (h_z and O_z), orientation, and $\Delta \phi$ is the rotational error within the marked surface.

When \vec{O}_z and \vec{h}_z coincide, the following formula is used.

$$\Delta \phi = \cos^{-1}(\vec{O}_x \cdot \vec{h}_x)$$

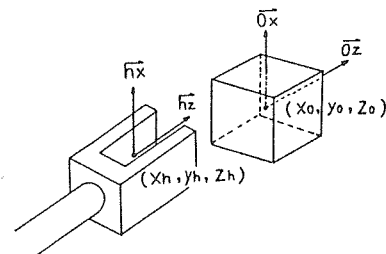


Fig. 7 Experimental conditions.

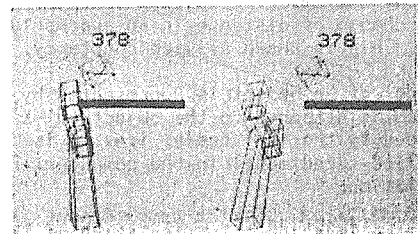


Fig. 8 Example of the displayed image.

(4) Effect of Presentation Time In order to determine an optimal presentation time, accuracy of the manipulation task is measured as a function of the presentation time. In this experiment binocular display with all possible cues were used. The average error for twenty trials were obtained. Figure 9 shows the result for the range error. Errors for the orientation and rotation showed the same tendency. That is, the error decreases as presentation time increases while it is less than 8 seconds. However, the same amount of error remains in spite of the increase of presentation time when it becomes more than 8 seconds. Therefore, an optimal presentation time of 9 seconds was used for the rest of the experiment.

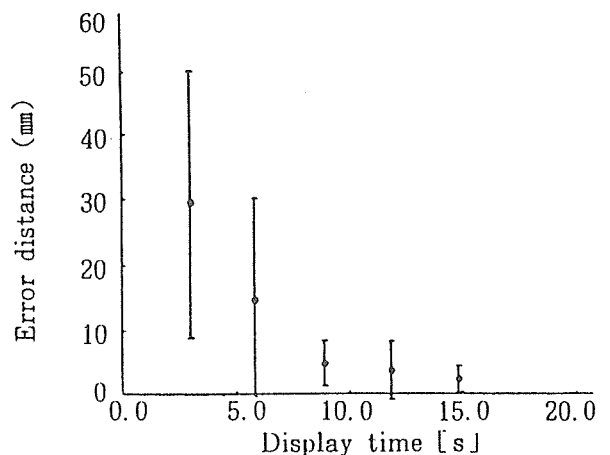


Fig. 9 Experimental results.
 - Effect of display time -

(5) Quantitative Comparison Table 1 shows the result for all possible combination of the display schemes. Average of twenty trials were indicated in the table. In the table it is become clear that the binocular display is superior to the monocular display scheme. This is quite apparent for the range detection. The same tendency was observed when additional range information was added. The average range error for the binocular display was half(0.5) of that for the monocular display. The average orientational error for the binocular display was 0.8 of that for the monocular display. The ratio for the rotational error was also 0.8. In the monocular display addition of bar-graphs mostly improved the result, while addition of the tone burst improves the orientational and rotational error. Addition of numerals were found to be less effective.

Solid Model vs. Wire-frame Model

Effect of the use of a solid model compared with a wire-frame model was examined under binocular presentation condition. Various orientation of the manipulator hand was randomly presented for a short time. A human subject was asked to memorize the presented orientation and try to reproduce the same orientation after he memorized the orientation. He controlled the displayed manipulator hand by moving his hand to attain the same orientation he memorized.

Figure 10 shows an example display of the solid model manipulator hand used in the experiment. Display distance was fixed to 500 mm. Orientational error of the reproduced orientation from the original orientation was compared for the case of solid model and wire-frame model as a function of presentation (display) time. In the figure the mark ■ indicates the result for the solid model while ● is for the wire-frame model. Each mark represents the average of ten runs. The result showed the preference of the solid model.

Electromagnetic Posture Sensor vs. Joystick

Effect of the use of the electromagnetic posture sensor as an input device was evaluated as compared with the use of a conventional joystick with three degrees of freedom.

Two figures which have the shape of numeral 4 and have different colors were displayed at the distance of 500 mm in front of a human subject (Fig. 12). One of the figures (4a) changes its orientation in all three directions randomly. The human operator controls the other figure (4b) using either the posture sensor or

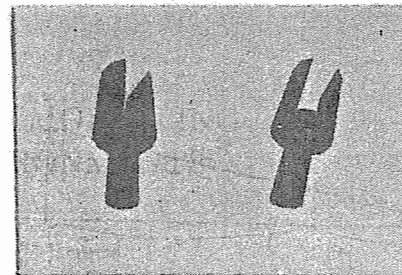


Fig. 10 Example of the solid model display.

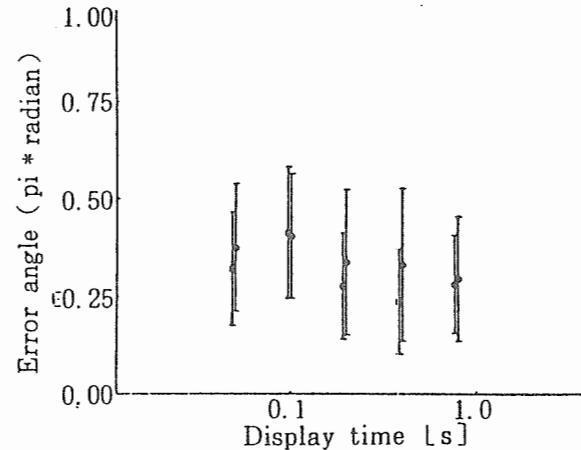


Fig. 11 Experimental results.
- comparison between the solid model (■) and wire-frame (●) -

the joystick. The subject was asked to follow the orientation of the randomly moving figure 4a controlling the other figure 4b to coincide with 4a.

The control system is described as a tracking system shown in Fig. 13 (a). The transfer function of the human operator with the input device T(f) is estimated as follows:

$$T(f) = \frac{\Phi_{xy}}{\Phi_{xz}} = \frac{\Phi_{iy}}{\Phi_{iz}} = \frac{E\{I(f) * \{O(f) + N(f)\}\}}{E\{I(f) * E(f)\}} = \frac{E\{I(f) * O(f)\}}{E\{I(f) * E(f)\}} = \frac{O(f)}{E(f)}$$

where \bar{X} is the cross spectrum between signals $x(t)$, $y(t)$, $i(t)$, and $z(t)$ which are indicated as subscripts. The signals $x(t)$, $y(t)$, and $z(t)$ are measured during finite time in order to determine their Fourier transforms. Upper case letters denote the Fourier transform of the corresponding lower case letters. The asterisk denotes the complex conjugate. E indicates an ensemble mean.

Figure 13 (b) shows an example of the transfer function obtained. As criteria for transfer function comparison the frequency (fc) where phase delay reaches -180 degrees and the root mean square error of the tracking (dc) are used.

Table 2 shows the result. It is clear from the table that the characteristics of the operator for the orientational tracking using the posture sensor is almost the same as that with the three axis joystick.

With the joystick, position can not be assigned when it is used to control both distance and orientation, while the posture sensor can assign both position and orientation at the same time. This means the superiority of the posture sensor to the joystick.

sub-display \ main-display		numeric bar-graph	pitch	no-aid	
stereo view	(error)				
	Δd (mm)	22.7	10.4	15.0	24.6
	$\Delta \theta$ (°)	11.7	15.8	8.45	10.0
	$\Delta \phi$ (°)	5.14	8.69	6.10	5.25
monocular view	Δd (mm)	48.3	18.9	35.7	35.7
	$\Delta \theta$ (°)	12.1	14.7	16.1	15.3
	$\Delta \phi$ (°)	15.0	5.85	6.40	12.4

Table 1 Comparison among several display schemes.

